ARTICLE

CircVPS13C promotes pituitary adenoma growth by decreasing the stability of IFITM1 mRNA via interacting with RRBP1

Weiyu Zhang[1,2,8], Siyu Chen[1,8], Qiu Du[1,3,8], Piaopiao Bian[1,4], Yutong Chen[5], Zexian Liu[6], Jian Zheng[6], Ke Sai[1], Yonggao Mou[1], Zhongping Chen[1], Xiang Fan[2]✉ and Xiaobing Jiang[1,7]✉

CircRNAs play important roles in a variety of biological processes by acting as microRNA sponges and protein scaffolds or by encoding functional proteins. However, their functions and underlying mechanisms remain largely unknown. Distinctive circRNA patterns were explored by comparing nonfunctioning pituitary adenomas (NFPAs) and normal pituitary tissues with a circRNA array. The biological functions of selected circRNAs were determined in vitro and in vivo. RNA-seq and circRNA pulldown assays were applied to investigate the underlying mechanisms. The circRNA profile of NFPAs is tremendously different from that of normal pituitary tissues. CircVPS13C is significantly upregulated in NFPA samples and cell lines. Gain- and loss-of-function experiments demonstrate that silencing circVPS13C inhibits the proliferation of pituitary tumor cells in vitro and in vivo. Mechanistically, circVPS13C silencing increases the expression of IFITM1 and subsequently activates its downstream genes involved in MAPK- and apoptosis-associated signaling pathways. Rescue experiments show that IFITM1 overexpression partly reverses the biological effects of circVPS13C. Further studies reveal that circVPS13C inhibits IFITM1 expression through a novel mechanism mainly by competitively interacting with RRBP1, a ribosome-binding protein of the endoplasmic reticulum membrane, and thereby alleviating the stability of IFITM1 mRNA. Clinically, circVPS13C expression is markedly higher in high-risk NFPA samples and is downregulated in patient serum 7 days post-transsphenoidal adenoma resection. Our findings suggest that circVPS13C is a critical regulator in the proliferation and development of NFPAs through a novel mechanism, whereby regulating mRNA stability via interacting with ribosome-binding proteins on the endoplasmic reticulum membrane.

Oncogene (2022) 41:1550–1562; https://doi.org/10.1038/s41388-022-02186-0

INTRODUCTION

Pituitary adenomas are among one of the most common intracranial tumors and have increased to 115 cases per 100,000 population over the past several decades, probably as a result of enhanced awareness and improved diagnostic imaging [1]. Approximately 30–40% of these cases are clinically nonfunctioning pituitary adenomas (NFPAs), which are characterized by a lack of hormonal secretion [2, 3]. According to the 4th edition of the World Health Organization classification of endocrine tumors, NFPAs can be categorized into eight subtypes: silent gonadotroph, corticotroph, somatotroph, thyrotroph, lactotroph, plurihormonal Pit-1, null-cell, and double/triple NFPAs [4]. Among them, silent corticotroph adenomas are recognized as high-risk pituitary adenomas [4]. Patients with NFPAs usually suffer from headache, visual field defects, and even hydrocephalus due to mass effects [5]. Moreover, NFPAs are the most frequent cause of hypopituitarism, which has been proven to be associated with overall excess mortality compared with that of the general population [6]. Surgical resection is currently the main treatment method. However, 16–30% of these patients relapse postoperatively [5]. Medical treatment and early detection of pituitary tumors could be potentially effective alternatives for preventing and managing invasive NFPAs. However, the development of these strategies has been hampered by the limited understanding of the mechanisms underlying pituitary tumorigenesis and development.

Unlike the functioning pituitary adenomas, very few gene mutations are associated with sporadic NFPA development, and genetic evaluation is rarely helpful for NFPA management [7]. Increasing studies have suggested that epigenetic modulation is tightly associated with the development of NFPAs [8]. Circular RNAs (circRNAs) represent a novel class of noncoding RNAs that are abundant and highly conserved in mammals. Aberrant expression patterns of circRNAs have been implicated in a variety of physiological and pathological processes [9–11]. CircRNAs are primarily known to act as competing endogenous RNAs or microRNA (miRNA) sponges to regulate transcriptional activity [12]. Our previous research found that circOMA1 promotes NFPA progression by acting as a sponge of the tumor suppressor miR-145–5p [13]. More recently, studies

[1]Department of Neurosurgery/Neuro-oncology, Sun Yat-sen University Cancer Center. State Key Laboratory of Oncology in South China, Collaborative Innovation Center for Cancer Medicine, Guangzhou, China. [2]Department of Neurosurgery, The Fifth Affiliated Hospital of Sun Yat-sen University, Zhuhai, China. [3]Department of Neurosurgery, The Affiliated Hospital of Yangzhou University, Yangzhou, China. [4]Department of Pathology, The Third Affiliated Hospital of Guangzhou Medical University, Guangzhou, China. [5]Department of Abdominal Oncology, cancer center of the Fifth Affiliated Hospital of Sun Yat-sen University, Zhuhai, China. [6]State Key Laboratory of Oncology in South China, Collaborative Innovation Center for Cancer Medicine, Guangzhou, China. [7]Department of Neurosurgery, Jiangmen Central hospital, Jiangmen, China. [8]These authors contributed equally: Weiyu Zhang, Siyu Chen, Qiu Du. ✉email: xiangfan@msn.com; jiangxiaob1@sysucc.org.cn

Received: 20 July 2021 Revised: 20 December 2021 Accepted: 10 January 2022
Published online: 28 January 2022

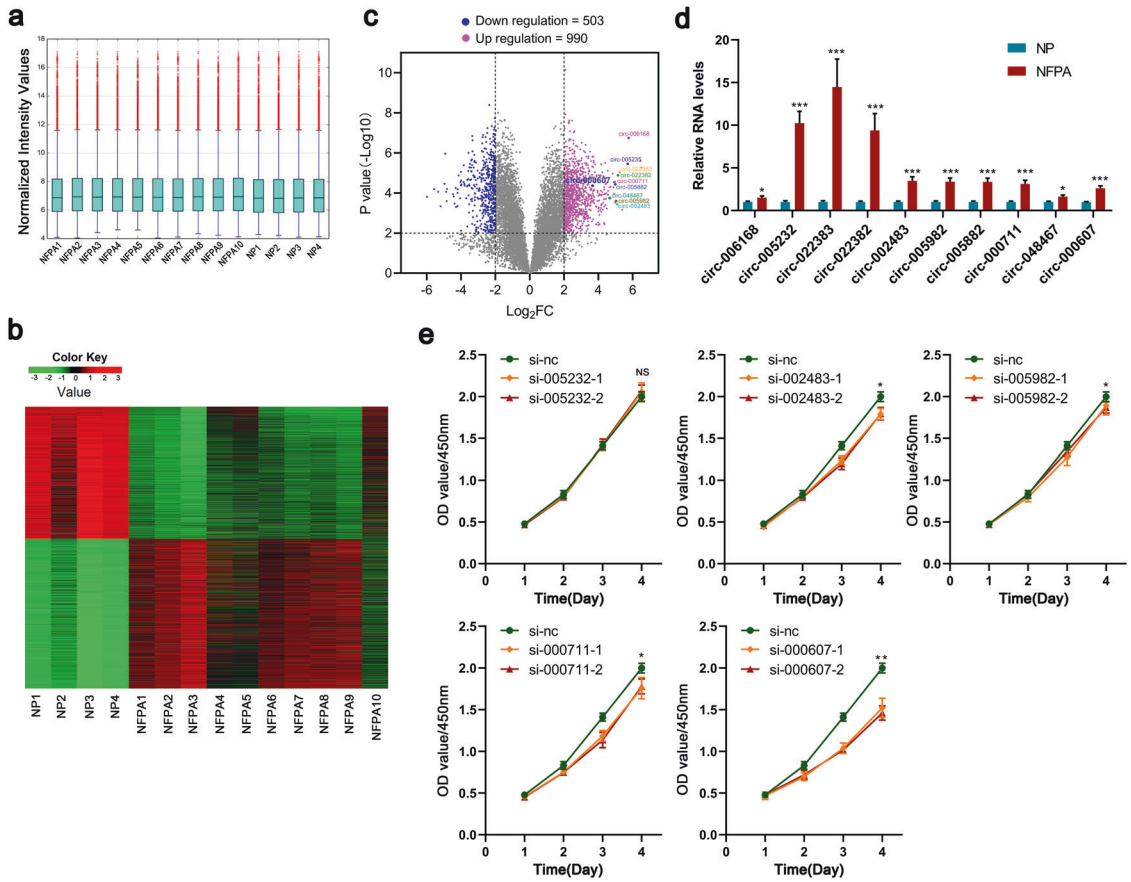

Fig. 1 Differential circRNA expression between NFPA ($n = 10$) and NP tissues ($n = 4$) and significantly increased circVPS13C expression in NFPA samples. Boxplots of microarray intensity values (**a**), heat map (**b**) and volcano plots (**c**) were used to display the expression profiles of circRNAs in the two groups (fold change≥4, FDR < 0.01). **d** Relative expression of ten selected circRNAs in NFPA and normal pituitary (NP) samples, as evaluated by qRT-PCR. **e** CCK-8 assay was performed to evaluate the biological effects of selected circRNAs on PDFS cells.

revealed that circRNAs could have roles in tumor progression beyond acting as miRNA sponges [10]. For example, circPABPN1 was proven to decrease ABPN1 translation by competitively binding to and sequestering HuR [14]. Circ-Foxo3 can function as a scaffold to bind to p53 and MDM2, thus promoting MDM2-induced p53 ubiquitination and degradation [15]. Circ-Amotl1 was shown to facilitate STAT3 nuclear translocation to bind to the DNMT 3a promoter and promote DNMT 3a transcription [16]. These studies indicate that circRNAs could influence protein expression, biogenesis, and pathophysiological processes by binding, storing, and sequestering proteins to subcellular locations [11]. Moreover, certain endogenous circRNAs can be translated to form protein or peptide isoforms in biologically significant amounts [17, 18]. Therefore, investigating circRNA-protein interactions is a fascinating and exciting endeavor, and the exact underlying mechanisms need to be characterized.

In the present study, we identified a circRNA derived from the VPS13C gene, termed circVPS13C (hsa_circ_0000607), which is markedly upregulated in NPFA samples and promotes the proliferation and colony formation of NFPA cells. CircVPS13C decreases the stability of interferon-induced transmembrane protein 1 (IFITM1) mRNA by competitively interacting with ribosome-binding protein 1 (RRBP1), which can promote mRNA stability by recruiting mRNA to anchor in the endoplasmic reticulum [19, 20]. The results of this study revealed a novel mechanism whereby circRNAs regulate mRNA stability by interacting with ribosome-binding proteins on the endoplasmic reticulum membrane. To the best of our knowledge, this is the first study to reveal the interaction of circRNAs and endoplasmic reticulum proteins.

RESULTS

Differential circRNA expression between NFPA and NP tissues and significantly increased circVPS13C expression in NFPA samples

CircRNA expression profiles were compared between age- and sex-paired NFPA ($n = 10$) and NP tissues ($n = 4$) by using a circRNA microarray. The boxplots of microarray intensity values demonstrated low variation between samples, suggesting that the circRNA expression pattern was similar between the two groups (Fig. 1a). Heat map (Fig. 1b) and volcano plots (Fig. 1c) were used to display the differentially expressed circRNAs in the two groups. A total of 1493 circRNAs were differentially expressed between the two groups (fold change ≥ 4, FDR < 0.01). Among them, 990 were significantly upregulated and 503 were significantly downregulated in the NFPA samples. We focused on upregulated circRNAs with higher absolute expression level, which could potentially be therapeutic targets and be more likely to be detected in tumor sample and serum.

Considering the fold change (>10), normalized relative abundance (>10), annotated genomic region (exonic) and FDR (<0.002), a total of 91 circRNAs were selected for further analysis. Then, ten of these circRNAs were chosen for further investigation because their parental genes have been reported to be involved in the regulation of cell proliferation. We examined the levels of these circRNAs in another 18 NFPA and 8 NP tissues by qRT-PCR, and all of them were confirmed to be significantly upregulated in NFPA samples compared to NP tissues (Fig. 1d). Then, the top five circRNAs with the lowest cycle threshold value of qRT-PCR were selected, and their biological function in pituitary tumor-derived

folliculostellate (PDFS) cells was evaluated with the CCK-8 assay. As shown in Fig. 1e, circVPS13C (circBase ID: hsa_circ_0000607) displayed the best inhibitory effect on cell proliferation when it was silenced. However, circRNAs silencing has none detectable effects on their parental linear genes (Fig. S1). Collectively, these results prompted us to investigate the role of circVPS13C in the occurrence and progression of NFPAs.

Identification and validation of circVPS13C in pituitary adenoma cells

CircVPS13C is transcribed from the VPS13C gene locus and is localized on human chromosome 15. It is 608 bp and contains exons 8–13. To confirm that circVPS13C is a circRNA, Sanger sequencing was performed to identify the head-to-tail splice junction (Fig. 2a). Then, divergent primers were designed to amplify the head-to-tail splicing site of endogenous circVPS13C using cDNA or gDNA extracted from PDFS cells as a template. The putative fragments were detected only with the cDNA template (Fig. 2b). Finally, RNase R resistance assay and agarose electrophoresis analysis confirmed that circVPS13C was resistant to RNase R, while GAPDH and linear VPS13C were sensitive (Fig. 2c). Taken together, these data confirmed that circVPS13C is a bona fide circRNA.

To characterize the subcellular location of circVPS13C, we performed costaining of circVPS13C with RNA-FISH assays and nucleoli with DAPI, in which circVPS13C was found to be enriched in both the cytoplasm and nucleoli in PDFS cells. Subcellular fractionation analysis followed by semiquantitative PCR further validated both the cytoplasmic and nuclear enrichment of circVPS13C (Fig. 2d). In addition, we detected the distribution of circVPS13C in NFPA and normal pituitary samples with RNA-FISH. In consistent with the finding of qRT-PCR, circVPS13C staining is more concentrated in NFPA samples than the one in normal pituitary tissues (Fig. 2e).

CircVPS13C silencing inhibits the proliferation of NFPA cells partly by increasing apoptosis

To evaluate the biological functions of circVPS13C in the development of NFPAs, gain- and loss-of-function experiments were performed by using both PDFS and human-derived NFPA primary cells. First, two back-splicing sequence-targeting shRNAs were designed to silence circVPS13C, and PDFS cells with stable expression of circVPS13C were also established. The results showed that circVPS13C expression was effectively silenced by both shRNAs and stably upregulated in PDFS cells transfected with the circVPS13C vector without a detectable effect on linear VPS13C expression (Fig. 3a). The CCK-8 assay revealed that circVPS13C silencing significantly impaired the proliferation of PDFS cells and human-derived NFPA cells, while circVPS13C overexpression had the opposite effects (Fig. 3b). Then, we further determined the effect of circVPS13C on another 6 human-derived NFPA primary cells. The CCK-8 assay showed that all of them were significantly inhibited by circVPS13C silencing at 72 h after culture (Fig. 3c). Similarly, the colony formation of PDFS cells was also significantly suppressed when circVPS13C was knocked down (Fig. 3d). Moreover, flow cytometry apoptosis assays showed that the fraction of apoptotic cells was significantly increased in cells with circVPS13C knockdown but decreased in cells overexpressing circVPS13C (Fig. 3e and Fig. S2a, b). Moreover, circVPS13C knockdown induced G0/G1 phase arrest (Fig. S2c) and inhibited cell invasion and migration (Fig. S2d–f).

To further prove the ability of circVPSC13C on pituitary adenoma cells, we evaluated the effect of circVPSC13C on the Mitogen-activated protein kinases (MAPK) signaling pathway, which has been shown to play crucial roles in cell proliferation of various tumors, including pituitary adenomas [21, 22]. Consistently, circVPS13C silencing decreased the protein levels of Bcl-2, phospho-ERK1/2 (p-ERK1/2), and phospho-P38 (p-P38) and increased the levels of cleaved Caspase-3, cleaved Caspase-9 and Bax in vitro. CircVPS13C overexpression exerted the opposite effects (Fig. 3f). Finally, to determine whether circVPS13C affects the proliferation of NFPA cells in vivo, we injected PDFS cells transfected with the circVPS13C expression vector or sh-circVPS13C into the subcutaneous tissue of nude mice. Tumors grown from circVPS13C-knockdown cells were significantly smaller and lighter than those grown from control cells (Fig. 3g). And the staining pattern of proteins related to apoptosis and MAPK signaling pathway in subcutaneous xenograft tumors is similar with the one from in vitro finding (Fig. S3). Taken together, these data suggest that silencing circVPS13C inhibits the proliferation of NFPA cells in vitro and in vivo, partly by increasing apoptosis.

CircVPS13C silencing inhibits cell proliferation partly by upregulating IFITM1 expression

Although most circRNAs are reported to function as sponges of miRNAs, their interactions with proteins are drawing increasing attention [11]. To investigate the potential mechanisms underlying the biological effects of circVPS13C on NFPA cells, we performed mRNA-seq analysis of three pairs of circVPS13C-silenced PDFS cells and control cells. The results showed that a total of 429 genes were significantly upregulated and 19 were downregulated after circVPS13C was silenced (Fig. 4a). The top ten genes with the most increased expression and nine genes with the most decreased expression were further verified in 15 NFPAs and 8 NP samples, and IFITM1 was one of the most significantly changed genes (Fig. 4b). Furthermore, the expression of IFITM1 was also significantly associated with circVPS13C in NFPA samples (Fig. S4). By reviewing the literature, we found that IFITM1 has been widely described to be involved in cell proliferation and migration [23–25]. Moreover, downregulated expression of IFITM1 was confirmed in 18 samples by western blot (Fig. 4c) and in 43 NFPA samples by qRT-PCR (Fig. S5a), and a significantly negative correlation was observed between circVPS13C and IFITM1 in the 43 NFPA samples (and Fig. 4d). Moreover, the IFITM1 level was negatively correlated with tumor size (Fig. S5b) and Knsop grade (Fig. S5c). Gain- and loss-of-function experiments showed that knockdown of circVPS13C increased IFITM1 expression, while circVPS13C overexpression produced the opposite results, as shown by qRT-PCR and western blotting in PDFS (Fig. 4e) and 6 human-derived NFPA primary cells (Fig. S5d). We used qRT-PCR to detect the expression of IFITM1 in xenograft tumor of PDFS with knockout or overexpression of circVPS13C, and the same result was obtained (Fig. S5e). Moreover, IFITM1 overexpression could significantly inhibit the proliferation of PDFS cells and induce cell apoptosis (Fig. S5f–h). To determine whether the biological effects of circVPS13C on NFPA cells were mediated by repressing IFITM1, a rescue assay involving circVPS13C and IFITM1 was performed. The results revealed that IFITM1 knockdown partly reversed the inhibition of cell proliferation and colony-forming ability induced by circVPS13C knockdown in PDFS cells (Fig. 4f–h). In addition, knockdown of IFITM1 partly reversed the effects of circVPS13C silencing on the levels of apoptosis-related proteins and proteins in the MAPK pathway (Fig. 4i). Collectively, these data suggest that circVPS13C silencing inhibits NFPA cell growth partly by enhancing IFITM1 expression.

By interacting with RRBP1, circVPS13C decreases the stability of IFITM1 mRNA, and thereby suppress its expression

We then attempted to investigate how circVPS13C modulates IFITM1 expression. The negative correlation between these molecules in NFPA samples indicated that circVPS13C is unlikely to regulate IFITM1 expression by sponging miRNAs. Furthermore, bioinformatic analysis showed that most of the potential miRNA targets of circVPS13C have only one or two binding sites. We thus speculated that circVPS13C might function through novel mechanisms beyond miRNA sponging. Recent evidence has revealed that circRNAs participate in molecular regulation by interacting with proteins [11]. First, we determined the influence of circVPS13C on the activity of the IFITM1 promoter. By performing a dual luciferase

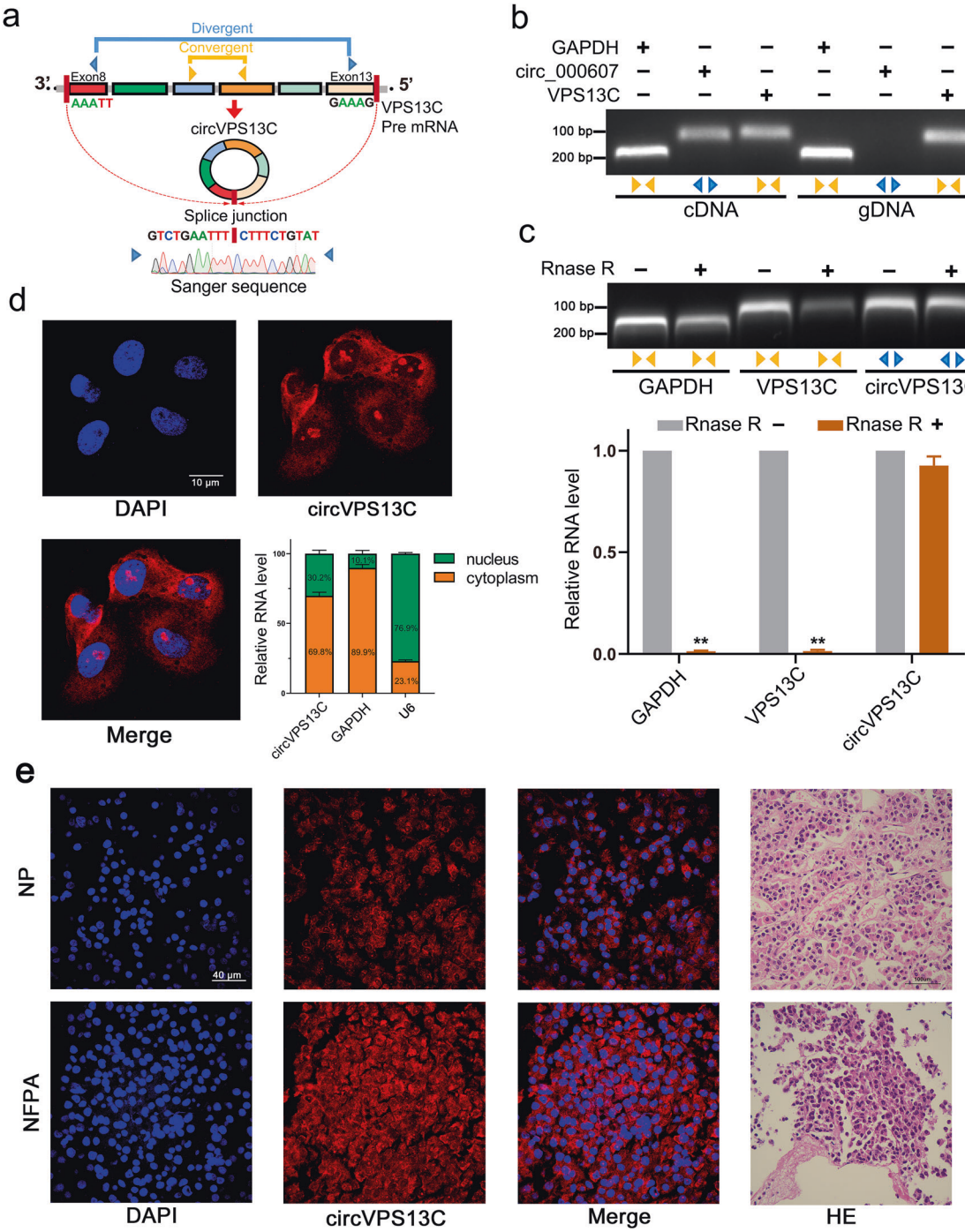

Fig. 2 Identification and validation of circVPS13C in pituitary adenoma cells. a Illustration of the annotated genomic region of circVPS13C, which was confirmed by Sanger sequencing. **b** Primers were designed to amplify the linear or back-splicing products using cDNA and genomic DNA (gDNA) extracted from PDFS cells as templates. **c** Total RNA from PDFS cells with or without RNase R treatment was subjected to qRT-PCR. **d** Costaining in RNA-FISH assays and nucleoli with DAPI indicates the cellular localization of circVPS13C. Relative expression of circVPS13C in the nucleus and cytoplasm was evaluated with qRT-PCR. GAPDH and U6 were used as reference genes. **e** RNA FISH assay was performed to detect the cellular localization and level of circVPS13C in pathologically defined NFPA and normal pituitary tissue.

reporter assay, we found that neither overexpression nor silencing of circVPS13C could induce detectable changes in IFITM1 promoter activity (Fig. S6a). We then hypothesized that circVPS13C might regulate IFITM1 expression via a posttranscriptional mechanism. Based on this hypothesis, we performed ChIRP assays to identify potential circVPS13C-associated proteins, as illustrated in Fig. 5a. The cell lysate of PDFS cells was incubated with biotin-labeled oligos to capture circVPS13C. CircVPS13C was then pulled down and purified with magnetic beads. As verified by ChIRP-qPCR, the enrichment efficiency of the circVPS13C-sense probe was 104-fold higher in the treated group than in the NC group (Fig. 5b). Agarose electrophoresis and silver staining were applied to identify circVPS13C RNA-related proteins, and we found a significantly different positive signal in the anti-circVPS13C probe group compared with the NC probe group. Then, LC-MS/MS assay was applied to identify the proteins in the positive sample (Fig. 5c).

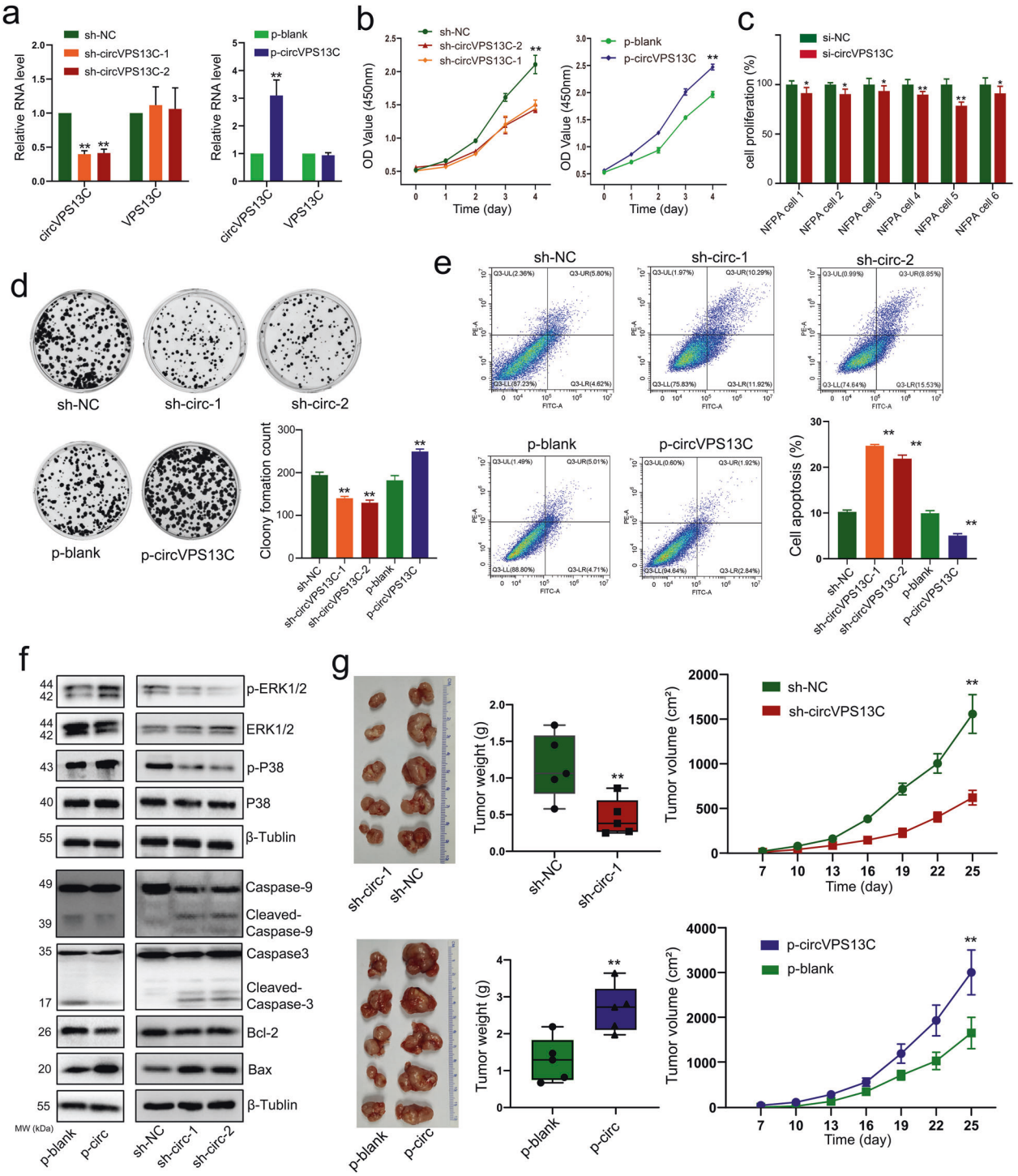

Fig. 3 Silencing of circVPS13C inhibits the proliferation of NFPA cells partly by increasing apoptosis. a PCR was performed to measure the level of circVPS13C in PDFS cells after treatment with two shRNAs and circVPS13C expression vectors. Silencing of circVPS13C inhibits the proliferation of PDFS (**b**) and human-derived NFPA cells (**c**), as shown by CCK-8 assays. **d** CircVPS13C promotes the growth of PDFS cells, as demonstrated by colony formation assays. **e** Silencing of circVPS13C induces apoptosis of PDFS cells, and circVPS13C expression inhibits apoptosis. **f** The key molecules of the MAPK pathway and apoptosis pathway were analyzed by western blotting. Silencing of circVPS13C decreases the protein levels of Bcl-2, phospho-ERK1/2 (p-ERK1/2) and phospho-P38 (p-P38) and increases the levels of cleaved Caspase-3, cleaved Caspase-9, and Bax. CircVPS13C overexpression exerts the opposite effects. **g** Xenograft tumor models show that tumors grown from circVPS13C-knockdown cells are significantly smaller and lighter than those grown from control cells.

Among the proteins enriched in the circVPS13C-sense probe group, RRBP1 (also known as p180), is of particular interest due to its top expression in the circVPS13C-sense probe group, since RRBP1 has been reported to be associated with the development of various malignant tumors (Fig. 5d) [26, 27]. We further confirmed the result with ChIRP-western blot analysis (Fig. 5d). Meanwhile, a significant positive correlation between IFITM1 and RRBP1 expression in 43 NFPA tissues was detected by qRT-PCR

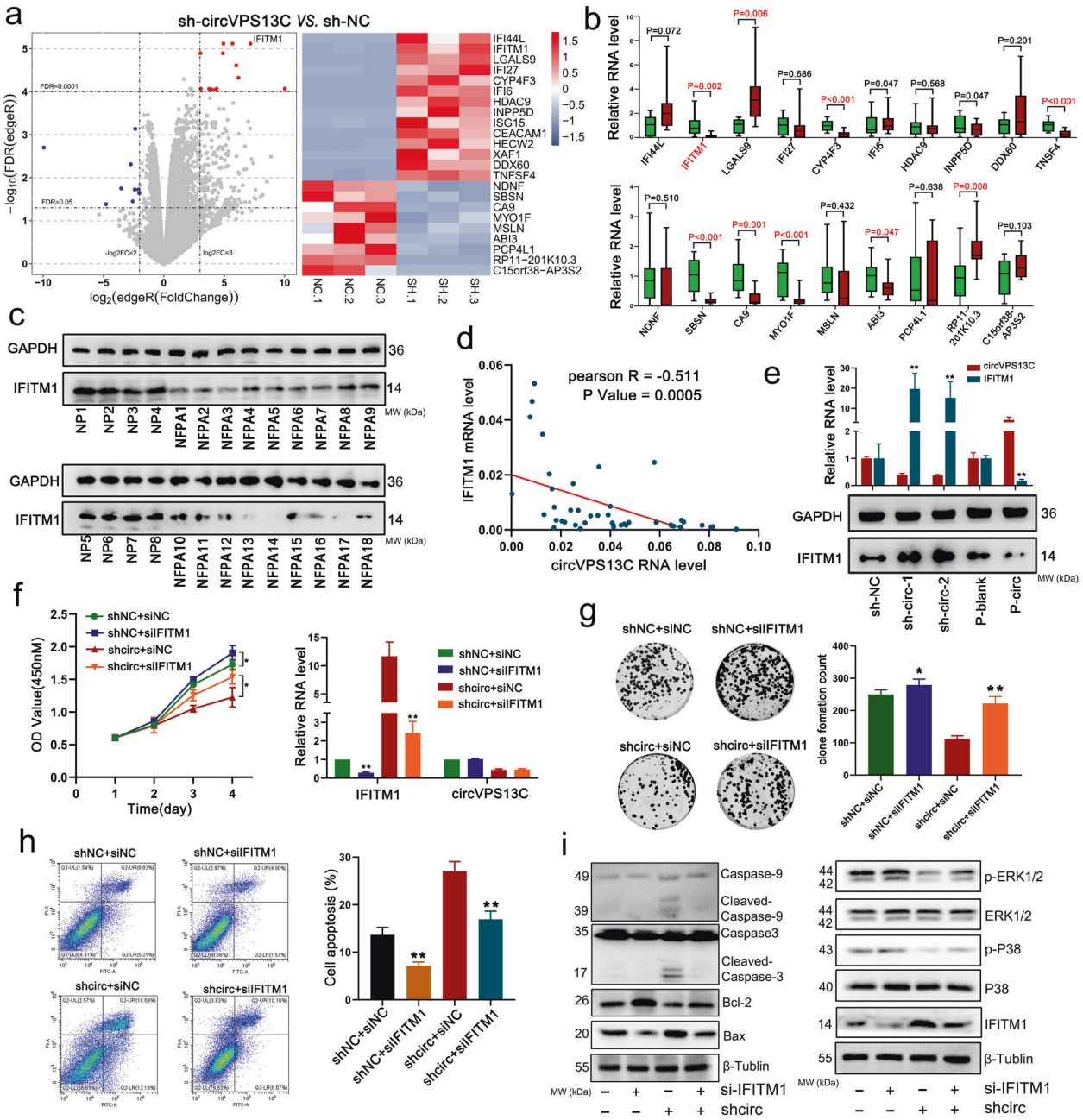

Fig. 4 Silencing of circVPS13C inhibits cell proliferation partly by upregulating IFITM1 expression. a mRNA-seq analysis of three pairs of PDFS circVPS13C-knockdown cells and control cells. **b** Genes with the most significant differences were evaluated in more NFPA ($n = 15$) and NP ($n = 8$) samples by qRT-PCR, and IFITM1 was identified as one of the most significantly upregulated genes after circVPS13C knockdown. **c** Decreased expression of IFITM1 in NFPA samples was confirmed by western blotting. **d** IFITM1 is negatively correlated with circVPS13C in a cohort of 43 NFPA samples. **e** Knockdown of circVPS13C increased IFITM1 expression, while circVPS13C expression produced the opposite results, as shown by qRT-PCR and western blotting. Knockdown of IFITM1 partly reverses the effects of circVPS13C silencing on cell growth and apoptosis, as demonstrated by the CCK-8 assay (**f**), colony formation assay (**g**) and flow cytometry (**h**). **i** Knockdown of IFITM1 partly reverses the effects of circVPS13C silencing on the levels of apoptosis-related proteins and proteins in the MAPK pathway.

(Fig. S6b). Then, we asked whether RRBP1 is involved in modulating the expression of IFITM1. As demonstrated in Fig. 5e, both IFITM1 mRNA and protein levels were markedly decreased after RRBP1 was silenced but increased in RRBP1-overexpressing cells, without a significant change in circVPS13C levels. Similarly, as confirmed by western blotting, RRBP1 overexpression increased IFITM1 levels and partly rescued the suppression of IFITM1 expression by circVPS13C (Fig. 5f). Previous studies have verified that RRBP1 is a protein located on the endoplasmic reticulum membrane that can regulate mRNA stability and enhance mRNA binding with ribosomes to promote translation [19, 28]. After the cells were treated with actinomycin D to suppress transcription, total RNA was extracted at different times for qPCR to detect the stability of IFITM1 mRNA. The results showed that degradation of IFITM1 mRNA was significantly accelerated when RRBP1 was silenced or circVPS13C was overexpressed. Overexpression of RRBP1 partly abolished the effects of circVPS13C on IFITM1 mRNA (Fig. 5g). Taken together, these data suggested that circVPS13C may regulate IFITM1 expression partly by interacting with RRBP1.

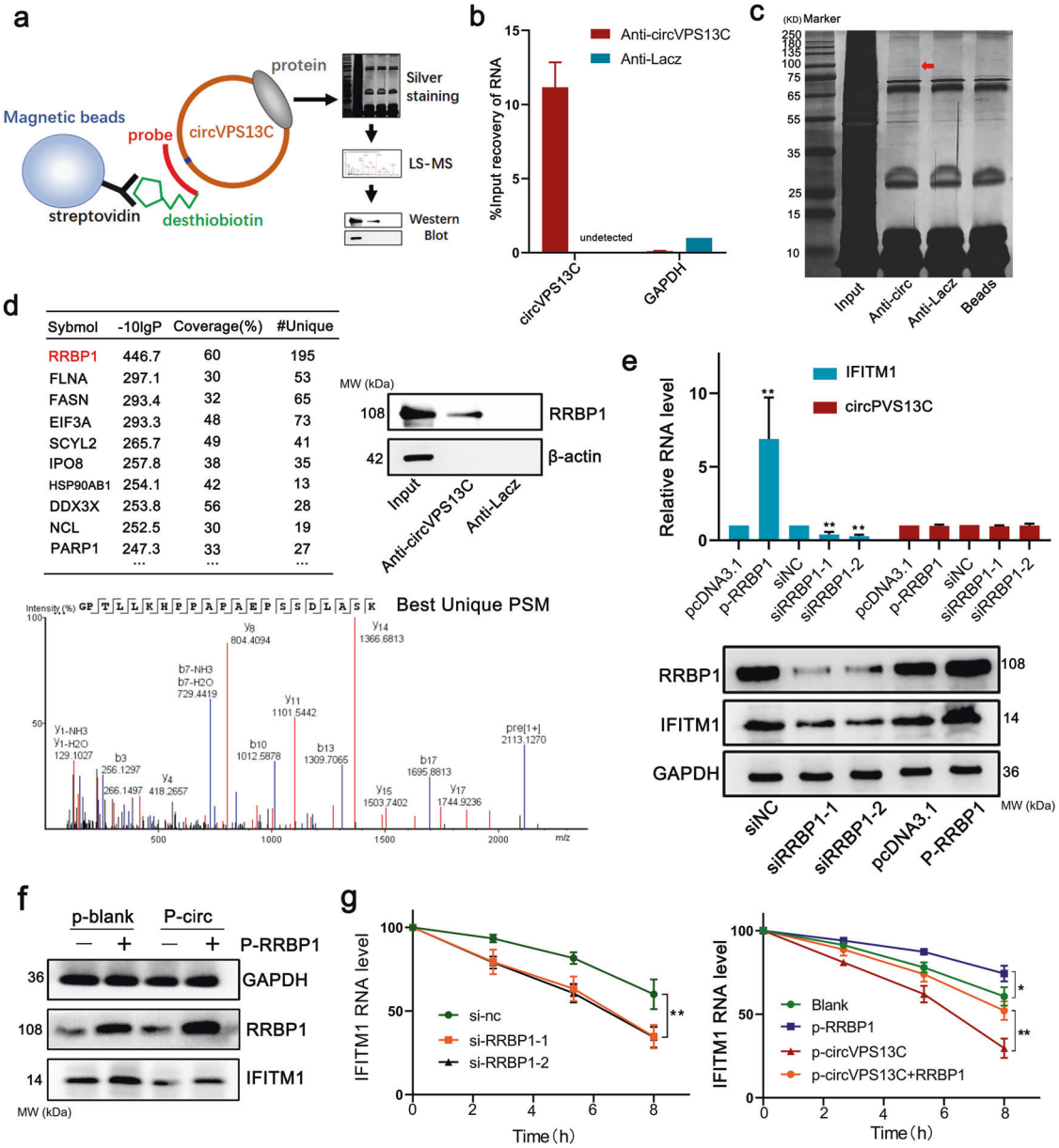

Fig. 5 CircVPS13C alleviates the stability of IFITM1 mRNA by interacting with RRBP1. a Schematic illustration of chromatin isolation by RNA purification (ChIRP) assays used to identify potential circVPS13C-associated proteins. **b** ChIRP-qPCR data indicate the enrichment efficiency of the circVPS13C-sense probe. **c** Agarose electrophoresis and silver staining show a different positive band in the anti-circVPS13C probe group compared with the NC probe group. **d** LC-MS/MS was applied to identify the proteins in the positive band, and RRBP1 was shown to have the best unique peptide spectrum match (PSM) and confirmed with ChIRP-western blot analysis. **e** Knockdown of RRBP1 decreases IFITM1 expression, while overexpression of RRBP1 produces the opposite results, as demonstrated by qRT-PCR and western blotting. **f** Overexpression of RRBP1 partly reduces the effects of circVPS13C on IFITM1. **g** After treated with actinomycin D, total RNA was extracted at different times for qPCR to detect RNA stability. RNA stability assay indicates that degradation of IFITM1 mRNA is significantly accelerated when RRBP1 is silenced or circVPS13C is overexpressed. Overexpression of RRBP1 partly abolishes the effects of circVPS13C on IFITM1 mRNA.

CircVPS13C suppresses IFITM1 expression by competitively interacting with RRBP1

Then, we asked how circVPS13C interacts with RRBP1 to suppress IFITM1 expression. Gain and loss of circVPS13C expression did not induce significant changes in RRBP1 protein levels (Fig. 6a). Similarly, RRBP1 and circVPS13C mRNA expression had no significant correlation in NFPAs samples ($n = 43$) (Fig. S6b). These data suggest that circVPS13C is unlikely to regulate RRBP1 expression. The RIP-qPCR results demonstrated that circVPS13C overexpression increased the level of circVPS13C and RRBP1 interaction, but decreased the one of IFITM1 and RRBP1 interaction, along with reduced IFITM1 mRNA expression. CircVPS13C silencing exerted the opposite effects. We thus concluded that circVPS13C suppress IFITM1 expression by competitively interacting with RRBP1 (Fig. 6b, c).

To declare the interaction between circVPS13C and RRBP1 protein, we firstly analyzed the potential binding sites of simulated structure for RRBP1-circVPS13C complex through RING software [29], and the results indicated that K51, E473, K474, Q479, Q551, T554, and T600 might be critical for the interaction. Then, the following mutant RRBP1 protein plasmids, RRBP1T554A + Q551A-flag (T554A), RRBP1T600A-flag (T600A), RRBP1Q479A + K474A + E473A-flag (Q479A) and RRBP1K51A-flag (K551A) were constructed. Specific antibodies were used to against flag tag,

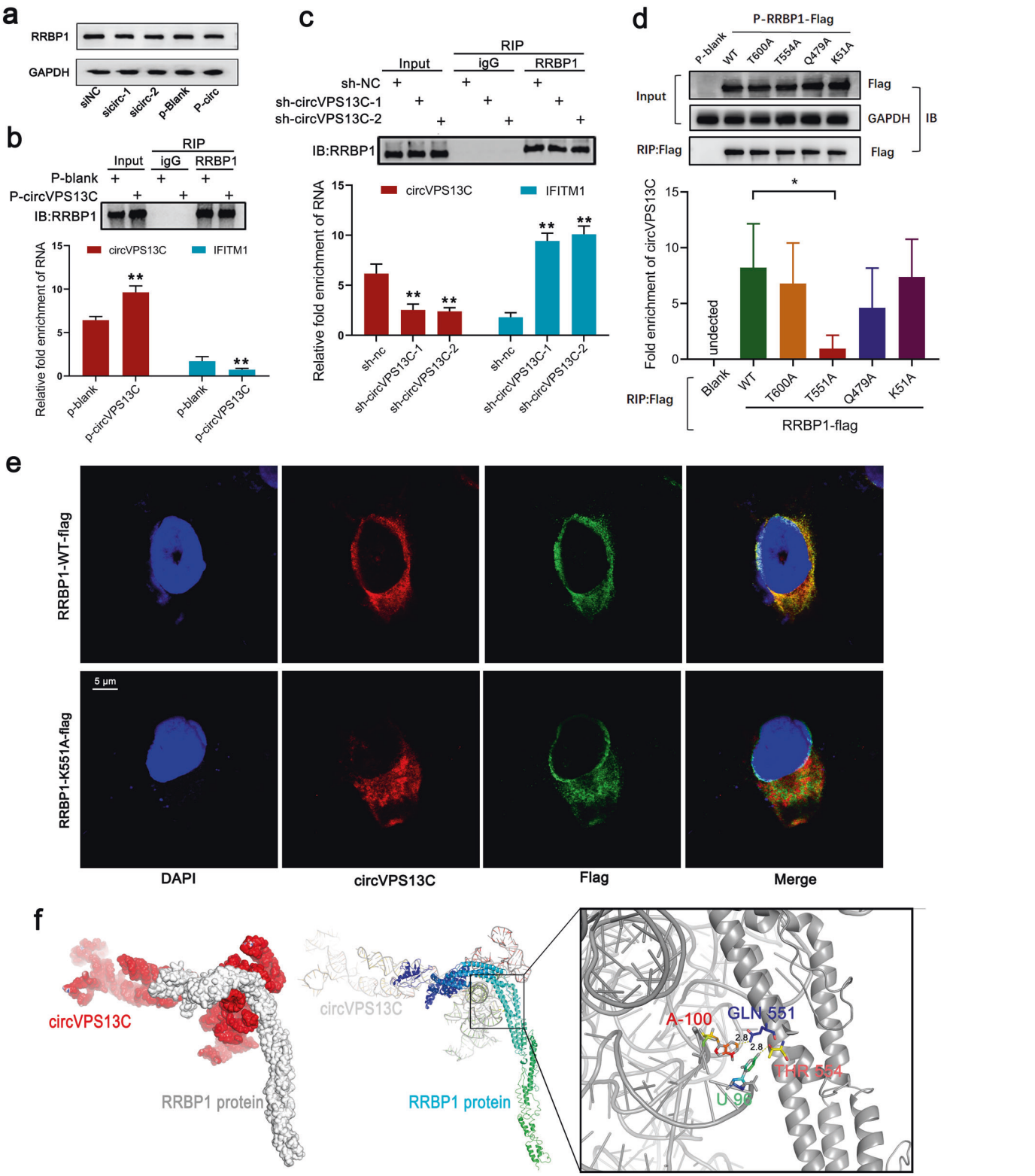

Fig. 6 CircVPS13C suppresses IFITM1 expression by competitively interacting with RRBP1. a Knockdown or overexpression of circVPS13C did not affect the expression level of the RRBP1 protein confirmed with western blot analysis. **b** RNA-binding protein immunoprecipitation (RIP) demonstrates the interaction between RRBP1 and circVPS13C in PDFS cells. RIP-qPCR results indicate that circVPS13C overexpression increased the interaction level of circVPS13C and RRBP1 but decreased the interaction level of IFITM1 mRNA and RRBP1. **c** Silencing of circVPS13C produced the opposite effects. **d** RRBP1T554A + Q551A(T554A) and circVPS13C interaction level decreased significantly compared to the one of RRBP1WT(WT) and circVPS13C, but there was no statistical significance in those of circVPS13C and RRBP1T600A(T600A), RRBP1Q479A + K474A + E473A(Q479A) or RRBP1K51(K51A) confirmed with RIP-qPCR. **e** Fluorescence colocalization results showed that circVPS13C and RRBP1WT protein colocalize in the cytoplasm of PDFS cells, but there was no detectable colocation with RRBP1T554A + Q551 (T554A). **f** Molecular docking diagram of circVPS13C and RRBP1.

following transfection of mutant RRBP1 and wild-type RRBP1 (WT) plasmids. RIP-qPCR results showed that RRBP1T554A + Q551A and circVPS13C interaction level decreased significantly compared to the one of RRBP1WT and circVPS13C, but there was no statistical significance in those of circVPS13C and RRBP1T600A, RRBP1Q479A + K474A + E473A or RRBP1K51 (Fig. 6d). We then transfected PDFS cells with plasmids of RRBP1T554A + Q551A and RRBP1WT for colocalization assays. Fluorescence colocalization results showed that circVPS13C and RRBP1WT protein colocalize in the cytoplasm of PDFS cells, but there was no detectable colocation with RRBP1T554A + Q551 (Fig. 6e). These results suggest that RRBP1 interacts with circVPS13C through residues including GLN551 and THR554. The simulated structure of the RRBP1-circVPS13C complex and the detailed residue interactions were visualized in Fig. 6f

Clinical significance of circVPS13C in NFPAs

The level of circVPS13C was evaluated in 93 NFPAs and 23 age- and sex-paired NP tissues by qRT-PCR (Table S1). As shown in Fig. 7a, the circVPS13C level was significantly increased in NFPA tissues compared with normal tissues, and upregulation of circVPS13C expression was demonstrated in almost all NFPA samples. However, the level of circVPS13C expression was not significantly changed in GH secreting adenomas ($n = 15$) and prolactinomas ($n = 26$), but downregulated in TSH adenomas ($n = 11$), compared to normal pituitary tissues (Fig. 7b).

Clinical factors influence circVPS13C expression were also analyzed. Much greater upregulated expression of circVPS13C was noted in the Knosp's grade IV samples (Fig. 7c) and the larger tumors (Fig. 7d). Silent corticotroph adenomas are recognized as high-risk pituitary adenomas [4]. We found that the average circVPS13C expression was significantly higher in silent corticotroph adenomas than in the other tumors (Fig. 7e). However, there was no significant difference of circVPS13C level between the primary and recurrent tumors (Fig. S6c). These data suggested that upregulation of circVPS13C expression might be associated with the progression and invasiveness of NFPAs, which is accordance with in vitro findings (Fig. S2d–f).

More interestingly, circVPS13C expression was downregulated in patient serum 7 days post operation (Fig. 7f). Furthermore, serum circVPS13C level was correlated with the one in tumor samples, and significantly associated with tumor diameter (Fig. 7g). Meanwhile, supernatant circVPS13C level was significantly related to intracellular expression and culture time of PDFS cells (Fig. 7h). In summary, our findings suggest that circVPS13C specially binding to and sequestering RRBP1, decreasing the expression of IFITM1 through promoting degradation of IFITM1 mRNA thus ultimately promoting the proliferation of NFPAs (Fig. 7i).

DISCUSSION

CircRNAs have been widely recognized to be involved in the pathogenesis and development of various tumors, including glioblastoma and breast, colon, and hepatocellular cancers [10]. However, the expression patterns and biological functions of circRNAs in pituitary adenoma development are not well known. The present study revealed a considerably different circRNA pattern between NFPA and NP tissues. CircVPS13C expression was found to be markedly upregulated and associated with aggressive features of NFPAs. CircVPS13C inhibits IFITM1 expression through a novel mechanism that mainly involves competitive interactions with RRBP1, a critical molecule in regulating endoplasmic reticulum stress. Our study reveals a new aspect of circRNA functions in development, whereby circRNAs recruit and bind endoplasmic reticulum proteins.

CircVPS13C was shown to be upregulated in NFPAs, but not GH secreting adenoma, prolactinoma, and TSH adenomas. Moreover, serum circVPS13C expression was significantly correlated with the one in tumor sample, and positively correlated with tumor diameter. These data indicate that serum circVPS13C might potentially act as an adjuvant biomarker for diagnosis and follow-up of NFPAs. However, it is far to demine the prognostic value for NFPAs. Much more prospective studies with larger samples and follow-up information are encouraged to declare this hypothesis. CircRNAs are generated by a "back-splicing" process, which is regulated by different cis-regulatory elements and trans-acting proteins [30]. All these elements may be involved in circVPS13C dysregulation in NFPAs. Recently, N6-methyladenosine modification was also suggested to modulate the expression of circRNAs [31]. Due to the design of this study, we did not explore the mechanisms regulating circVPS13C expression in NFAPs, which is to be declared in future studies.

To date, most functional circRNAs have been proposed to function as miRNA sponges in the cytoplasm. One of the best-known sponging circRNAs in humans is ciRS-7, which contains more than 70 selectively conserved binding sites for miR-7. It strongly suppresses miR-7 activity, resulting in increased levels of miR-7 targets [12]. However, only a few circRNAs contain multiple binding sites to trap one specific miRNA, and AGO2 PAR-CLIP data revealed that most circRNAs do not bind extensively to miRNAs [32]. Some circRNAs also serve as templates to produce biologically active protein or peptide isoforms [10, 33]. Recently, an increasing number of studies have identified multiple functions of circRNAs beyond their miRNA sponging and protein-coding abilities. Among them, the interactions between circRNAs and proteins are complicated and remain to be defined. RNA-binding proteins (RBPs) are the most common proteins that are known to interact with circRNAs, which, in turn, mediate the maturation, transport, and translation of proteins. CircRNAs could function as decoys to change the regular function of proteins [14] or as scaffolds facilitating the contact between two or more proteins [15]. In the present study, we found that circVPS13C decreased the expression of IFITM1 by recruiting RRBP1, which is a protein located on the endoplasmic reticulum membrane involved in regulating mRNA stability [19]. This is similar to the mechanism described by Chen et al., in which circRNA FECR1 modulates FL1 methylation by recruiting TET1 [34].

The IFITM family of genes encodes small homologous proteins localized in the plasma and endolysosomal membrane. To date, five IFITM genes have been identified in humans [35]. IFITM proteins have mostly been studied in terms of their immune functions, and IFITM members enable cells to be resistant to viral infections [25, 36]. However, IFITM proteins and their dysregulated expression have also been described to play an antiproliferative role by cell cycle control, apoptosis, and ERK pathway inhibition [23, 37], suggesting that these proteins may also play important roles in other diseases, such as cancers. Yu et al. found that increased IFITM1 expression in human colorectal cancer significantly correlated with a more advanced clinical stage and worse prognosis [38]. Similarly, elevated IFITM1 expression was confirmed in breast and oral cancers and was reported to be correlated with poor overall survival and chemotherapy resistance [39, 40]. In contrast to previous studies, in this investigation, IFITM1 expression was significantly decreased in NFPAs compared with normal pituitary tissue. Furthermore, overexpression of IFITM1 in NFPA cells inhibited, whereas knockdown of IFITM1 promoted, cell proliferation in vitro. The distinct role of IFITM1 in NFPAs from highly malignant tumors indicated that the tumor microenvironment is a vital determinant of IFITM1 function. Our study suggested a novel role of IFITM1 in proliferation and development, which deserves more attention in the future.

RRBP1 (also known as p180) is mainly localized on the endoplasmic reticulum membrane and is a critical molecule in regulating endoplasmic reticulum stress [27, 41]. RRBP1 overexpression can enhance the association of mRNAs with the

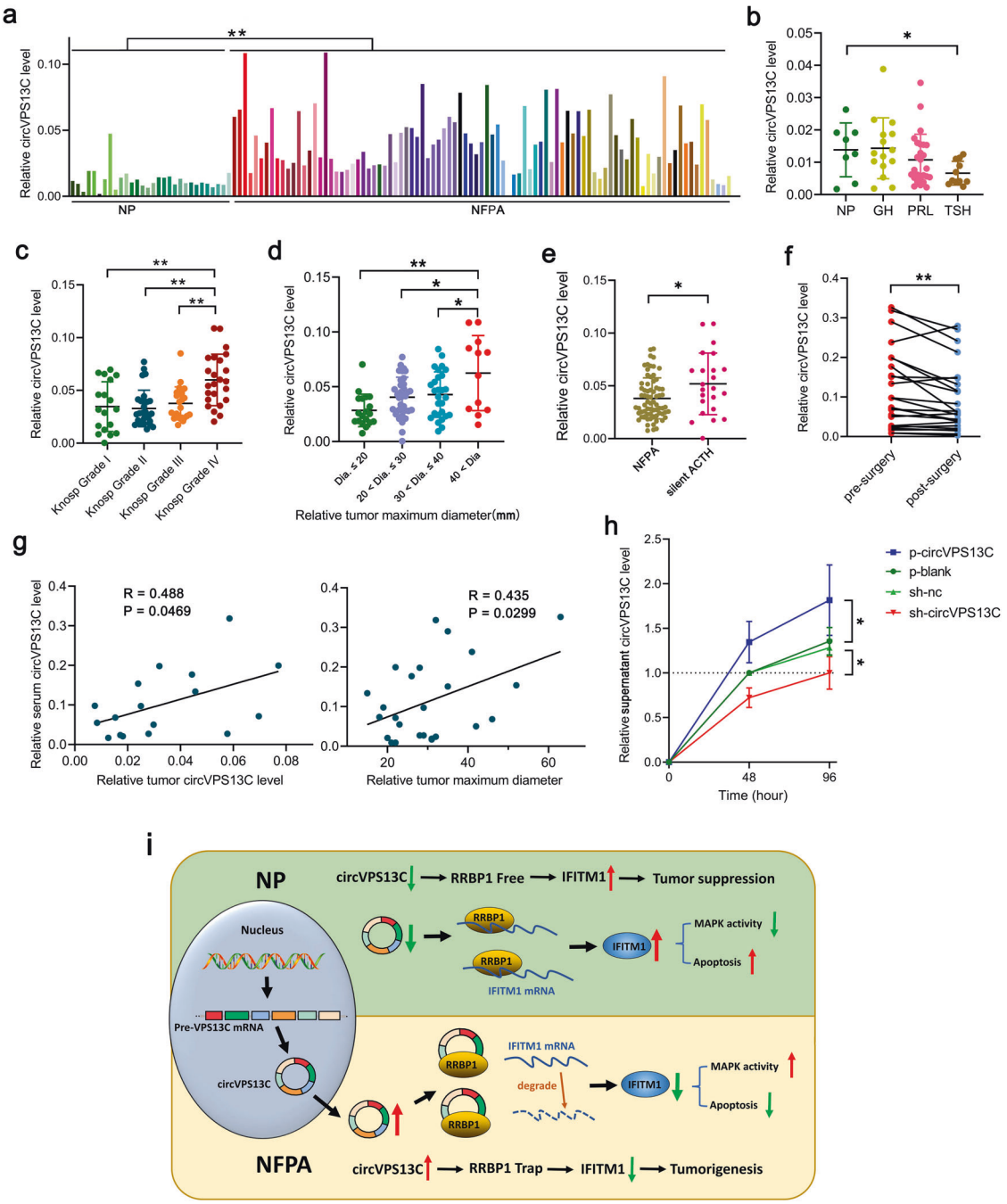

Fig. 7 Clinical significance of circVPS13C in NFPAs. a The level of circVPS13C was evaluated in 93 NFPAs and 25 age- and sex-paired normal pituitary tissues by qRT-PCR. **b** The level of circVPS13C was evaluated in 15 growth hormone-secreting pituitary adenomas (GH), 26 prolactin-secreting pituitary adenomas (PRL), 11 thyroid-stimulating hormone-secreting pituitary adenomas (TSH), and 8 normal pituitary tissues by qRT-PCR. **c** The level of circVPS13C was significantly higher in Knosp's grade IV samples than in the other tumor samples. **d** The level of circVPS13C in tumor samples with a maximum diameter larger than 40 mm was significantly higher than that in other tumor samples with smaller diameters. **e** The level of circVPS13C is significantly higher in silent corticotroph adenomas than in other adenomas. **f** The serum level of circVPS13C is significantly downregulated in NFPA patients 7 days post-transsphenoidal adenoma resection in a cohort of 25 patients. **g** Serum circVPS13C level was positively correlated with tumor size ($n = 25$) and the one in tumor samples in 17 patients with enough tissues for RNA extraction. **h** qRT-PCR was performed to measure circVPS13C level in cell culture supernatant of PDFS with knockdown or overexpression of circVPS13C. **i** Proposed model of circVPS13C repressing IFITM1 and promoting NFPA growth.

endoplasmic reticulum [20]. It can also regulate mRNA stability and enhance mRNA binding with ribosomes to promote translation by recruiting membrane proteins or secreted proteins to anchor in the endoplasmic reticulum [28]. In the present study, due to the increase in circVPS13C and RRBP1 interaction, the interaction of RRBP1 and IFITM1 was decreased, thus enhancing IFITM1 stability. Clinically, RRBP1 expression was frequently observed to be elevated in solid malignant tumors, including breast [42], colorectal [26], and lung cancers [27], and high RRBP1 predicted shorter disease-free survival [26, 42]. However, in the present study, RRBP1 seemed to function as a tumor suppressor, since it could increase the expression of IFITM1, which was shown to suppress the

proliferation of NFPAs. Moreover, we demonstrated that the stability of IFITM1 mRNA was decreased when the interaction of circVPS13C and RRBP1 was enhanced. Therefore, circVPS13C was predicted to function as a sponge of RRBP1, thus promoting the proliferation of NFPA cells by suppressing IFITM1 expression.

The present study also has some limitations. Firstly, circVPS13C displays impressive suppression on the proliferation of NFPA cells. Better in vivo and in vitro models, if possible, are warranted to further confirm our finding. Secondly, mechanisms regulating circVPS13C expression and the role of nucleus circVPS13C remain to be clarified in the future. Finally, more prospective studies with larger number of patients and longer follow-up period are encouraged to declared the prognostic value of circVPS13C for NFPAs.

CONCLUSIONS

CircVPS13C is significantly upregulated in NFPA samples and associated with aggressive features of NFPAs. Through competitive interactions with RRBP1, circVPS13C silencing decreases the stability of IFITM1 mRNA, thereby suppressing the growth of NFPA cells. CircVPS13C is a critical regulator in the proliferation and development of NFPAs, suggesting its potential role to be a diagnostic factor and therapeutic target for NFPA management.

METHODS

Human tissue samples

Pituitary adenomas with no clinical evidence of hormonal hypersecretion were considered as NFPAs [2, 3]. A total of 93 human clinically NFPA tissues were obtained from surgical resections of patients at the Department of Neurosurgery of Sun Yat-sen University Cancer Center from 2015 to 2019. The patient's clinical and pathological information has been uploaded to the online database. A total of 23 samples of human normal pituitary (NP) tissues were obtained from autopsy materials (healthy people who died accidentally without disease) from the Forensic Assurance Center of Sun Yat-sen University, where each sample was confirmed to be free of any previous pathologically detectable conditions by HE staining. Informed consent, including a tissue sharing clause, was obtained from a family member of the deceased individual before the autopsy. To rule out RNA degradation, NP RNA quantity and quality were assessed by a NanoDrop ND2000 (Thermo Fisher Scientific, Waltham, MA) before use, and RNA integrity was tested by denaturing agarose gel electrophoresis. The use of human tissues in the study was approved by the medical ethics committee of Sun Yat-sen University Cancer Center.

Cell culture

A PDFS cell line was a gift from the Neuroendocrine Unit, Massachusetts General Hospital, Harvard Medical School [43] and cultured in Dulbecco's modified Eagle's medium (DMEM)/high glucose supplemented with 10% fetal bovine serum (FBS) (Gibco, USA), 100 U/mL penicillin, and 100 μg/mL streptomycin. Primary tumor cells from NFPA tissues were isolated and cultured as described previously [13] and cultured in DMEM/F12 medium (Gibco, NY, USA) supplemented with 10% FBS. All cultured cells were maintained at 37 °C in a humidified atmosphere of 5% CO_2.

Animal experiments

Female nude mice (BALB/c-nu/nu), 4 weeks old and weighing approximately 12 g, were purchased from GemPharmatech (Jiangsu, China). All animals were housed under pathogen-free conditions with water and food provided ad libitum at 20–26 °C, 40–70% relative humidity, 15 times/h ventilation, and a 12 h light/12 h dark cycle. Mice were randomly assigned to a group of 5 and were subcutaneously injected with 5×10^6 PDFS cells in 100 μL serum-free DMEM. The tumor volume (V) was evaluated by measuring tumor length (L) and width (W) with vernier calipers and calculated using the formula $V = 0.52 \times L \times W2$. After 25 days, the mice were killed, and the tumor tissues were harvested.

RNA and genomic DNA (gDNA) extraction

Total RNA was extracted from cells or tissue using TRIzol reagent (Thermo Fisher Scientific, MA, USA) according to the manufacturer's instructions. In addition, gDNA was extracted using a gDNA isolation kit (Tiangen, Beijing, China).

RNase R treatment, cDNA synthesis, and PCR/qPCR

Aliquots of total RNA (2 μg) were incubated with or without 3 U/μg RNase R (cwbiotech, Beijing, China) for 30 min at 37 °C, and the RNA products were purified using an RNeasy MinElute cleaning kit (Qiagen, Germany). First, isolated RNA was reverse transcribed to cDNA using PrimeScript RT Master Mix (TaKaRa, Dalian, China). Then, PCR was performed using PrimeSTAR Max DNA Polymerase (TaKaRa, Dalian, China) according to the manufacturer's instructions. PCR products were subjected to electrophoresis on 2% agarose gels and visualized using Safe Green (Biosharp, China). qPCR was performed according to the manufacturer's instructions (Yesen, Shanghai, China) using a CFX96 Touch Real-Time PCR Detection System (Bio-Rad). To evaluate mRNA and circRNA expression, the qPCR results were normalized to GAPDH mRNA expression as the internal control using the $2^{-\Delta\Delta Ct}$ method. Sanger sequencing and primer synthesis were performed by Sangon Biotech (Shanghai, China). Primer sequences are provided in the Additional file.

CircRNA microarray

CircRNA expression profiles of NFPAs ($n = 10$) and NP tissues ($n = 4$) were compared by using a circRNA microarray (Arraystar human circRNA Array V2, Aksomics, China). Total RNA from each sample was quantified using a NanoDrop ND-1000. The sample preparation and microarray hybridization were performed based on Arraystar's standard protocols. Briefly, total RNA was digested with RNase R (Epicentre, Inc.) to remove linear RNAs and enrich circRNAs. Then, the enriched circRNAs were amplified and transcribed into fluorescent cRNA utilizing a random priming method (Arraystar Super RNA Labeling Kit; Arraystar). The labeled cRNAs were hybridized onto the Arraystar Human circRNA Array V2 (8×15 K, Arraystar). After washing the slides, the arrays were scanned by the Agilent Scanner G2505C. Agilent Feature Extraction software (version 11.0.1.1) was used to analyze the acquired array images. Quantile normalization and subsequent data processing were performed using the R software limma package. Differentially expressed circRNAs with statistical significance between two groups were identified through volcano plot filtering. Differentially expressed circRNAs between two samples were identified through fold change filtering. Hierarchical clustering was performed to show the distinguishable circRNA expression pattern among samples.

SiRNA, plasmid synthesis, and lentivirus infection

SiRNAs were synthesized by RiboBio (Guangzhou, China). Short hairpin RNA (shRNA) targeting circVPS13C was designed according to the siRNA sequence. Plasmid and the prepackaged lentivirus were purchased from GenePharma (Guangzhou, China) and used to infect PDFS cells according to the manufacturer's instructions, followed by puromycin (5 μg/mL) selection for 4 weeks. SiRNA sequences are provided in the Additional files.

Cell proliferation and colony formation assays

Cells were seeded at a density of 5×10^3 cells/well in 96-well plates and cultured for 24, 48, 72, and 96 h. Cell Counting Kit-8 (Dojindo Laboratories, Japan) reagent was used to measure cell proliferation according to the manufacturer's instructions. For colony formation assays, the cells were seeded at a density of 400 cells/well into each well of six-well plates and incubated for 14 days. Next, the colonies were fixed with 4% paraformaldehyde (Sigma-Aldrich, MO, USA) for 20 m and then stained with 0.1% crystal violet (Sigma-Aldrich, MO, USA) for 10 m. The colonies were imaged and counted.

Cell apoptosis assay, cell migration, and invasion assay

An Annexin V-FITC/PI Apoptosis Detection Kit (Keygen, Nanjing, China) was used to quantify cell apoptosis. Cells were seeded in six-well plates at a density of 1×10^6 cells/well and incubated for 24 h before transfection. After 48 h of culture, the cells were rinsed with phosphate-buffered saline (PBS) and centrifuged twice at 1,200 rpm for 3 m. The cells were resuspended in binding buffer and stained with Annexin V-FITC/PI according to the manufacturer's instructions. The apoptotic fraction was analyzed by a fluorescence-activated cell sorting flow cytometer (Beckman Coulter, Inc. Brea, CA, USA). Cell migration and invasion assay were performed with Transwell Chamber and Corning Matrigel Invasion Chamber, respectively [13].

Western blot analysis

Antibodies against IFITM1 (Cat# ab106265), GAPDH (Cat# ab8245), and RRBP1 (Cat#ab95983) were purchased from Abcam (USA). Antibodies against Phospho-p38 (Cat#4511), p38 (Cat#9212), Phospho-Erk1/2 (Cat#4370), Erk1/2 (Cat#4695), Cleaved Caspase-3 (Cat#9664), Caspase-3 (Cat#9662), Caspase-9 (Cat#9508), Bax (Cat#5032) and Bcl-2 (Cat#105071) were purchased from Cellsignal Technology (USA). Total proteins from cells or tissue were extracted using RIPA lysis buffer (CWBIO, Beijing, China), and the protein concentration was measured using a BCA assay kit (Invitrogen, USA). Proteins were separated using 10% SDS-PAGE and transferred to a 0.45 μm polyvinylidene fluoride (PVDF) membrane (Merck Millipore, USA). The PVDF membrane was blocked with 5% nonfat milk in PBS with Tween 20 at 37 °C for 1 h and incubated at 4 °C overnight with primary antibodies against the following antigens: IFITM1 (1:1000), GAPDH (1:3,000), RRBP1 (1:1000) and other antibodies (1:2000). The membranes were then incubated with horseradish peroxidase (HRP)-conjugated goat anti-mouse IgG (H + L) or HRP-conjugated goat anti-rabbit IgG (H + L) secondary antibody for 1 h at room temperature. The membranes were visualized with Immobilon ECL Ultra Western HRP Substrate (Merck, Shanghai, China) and a Bio-Rad ChemiDoc system (Bio-Rad, Shanghai, China).

Fluorescence in situ hybridization (FISH)

FISH was conducted in PDFS cells with CY3-labeled RNA fluorescence probes (GenePharma, Shanghai, China). Cells were fixed when they reached a confluency of 50–75%. After prehybridization according to the FISH kit instructions (GenePharma), the cells were hybridized with circVPS13C-specific CY3-labeled probe at 37 °C overnight. Then, the signal was detected under a confocal microscope. The probe sequence and CY3-labeled site are provided in the Additional file.

Chromatin isolation by RNA purification (ChIRP) and liquid chromatography tandem mass spectrometry (LC-MS/MS) analysis

A Magna ChIRP Kit (Millipore, MA, USA) and biotin-labeled circVPS13C probes (GenePharma, Shanghai, China) were used to pulldown circVPS13C and its binding protein. First, cells were lysed with lysis buffer supplemented with protease inhibitor and 1 U/μL RNase inhibitor (Thermo Fisher Scientific) on ice for 30 min with occasional mixing. Second, the probes or negative control (NC) probes were added to the lysate at 37 °C for 4 h. Third, streptavidin magnetic beads were mixed with the lysate at 37 °C for 1 h and washed with wash buffer five times. Finally, RNA was isolated and purified for qRT-PCR, and proteins were isolated and purified for silver staining, mass spectrometry, and western blotting. Silver staining analysis was performed using a silver stain kit (Beyotime Biotechnology, Shanghai, China) according to the manufacturer's instructions. LC-MS/MS detection and analysis were provided by Wininnovate Bio (Shenzhen, China). The probe sequence and biotin-labeled site are provided in the Additional file.

Actinomycin D assay

Cells were cultured with or without 2 μg/mL actinomycin D (Sigma-Aldrich, MO, USA) in medium. Then, the cells were harvested at different time points, followed by RNA extraction and qPCR detection of RNA stability, as described above.

Ribonucleoprotein immunoprecipitation (RIP)

A total of 1×10^7 cells were lysed with IP lysis buffer (Beyotime Shanghai, China). Cell extracts were incubated with an RRBP1 antibody (1 μg antibody/1 mg total cellular protein) or NC normal mouse IgG. The RRBP1 complex (RRBP1 protein, bound RNA, and RRBP1 antibody) was purified using Protein G Plus/Protein A agarose. The final proteins were digested using Proteinase K, and RNA was isolated and used for qPCR.

Molecular docking analysis

The protein structure of RRBP1 was predicted by I-TASSER (PMID: 25883148). The secondary structure of circVPS13C was predicted by the Vienna RNA web server (PMID: 12824340, 16452114) and then employed to predict 3D structure by 3dRNA (PMID: 28482022). The structure of the RRBP1-circVPS13C complex was modeled by HDOCK (PMID: 28521030) and visualized by PyMOL (https://pymol.org).

Statistical analysis

All experiments were performed at least in technical triplicates and in three independent biological repeats. Numerical data are presented as the mean ± SD. Student's *t* test was used to determine the statistically significant differences between the two groups. Analysis of variance was used to determine the statistically significant differences between three or four groups. Variance associations between circVPS13C and IFITM1 were determined using Pearson analysis. Statistical analyses were performed using SPSS statistical software, version 16.0 (IBM Corp., NY, USA). Values were considered statistically significant at $P < 0.05$.

DATA AVAILABILITY

Clinical information of samples and primers used in the present study can be found in supplementary tables. Other original data in our study are available upon request.

REFERENCES

1. Agustsson TT, Baldvinsdottir T, Jonasson JG, Olafsdottir E, Steinthorsdottir V, Sigurdsson G, et al. The epidemiology of pituitary adenomas in Iceland, 1955-2012: a nationwide population-based study. Eur J Endocrinol. 2015;173:655–64.
2. Aflorei ED, Korbonits M. Epidemiology and etiopathogenesis of pituitary adenomas. J Neurooncol. 2014;117:379–94.
3. Esposito D, Olsson DS, Ragnarsson O, Buchfelder M, Skoglund T, Johannsson G. Non-functioning pituitary adenomas: indications for pituitary surgery and post-surgical management. Pituitary. 2019;22:422–34.
4. Mete O, Lopes MB. Overview of the 2017 WHO classification of pituitary tumors. Endocr Pathol. 2017;28:228–43.
5. Melmed S. Pituitary-tumor endocrinopathies. N Engl J Med. 2020; 382:937–50.
6. Jasim S, Alahdab F, Ahmed AT, Tamhane S, Prokop LJ, Nippoldt TB, et al. Mortality in adults with hypopituitarism: a systematic review and meta-analysis. Endocrine. 2017;56:33–42.
7. Song ZJ, Reitman ZJ, Ma ZY, Chen JH, Zhang QL, Shou XF, et al. The genome-wide mutational landscape of pituitary adenomas. Cell Res. 2016;26:1255–9.
8. Yacqub-Usman K, Richardson A, Duong CV, Clayton RN, Farrell WE. The pituitary tumour epigenome: aberrations and prospects for targeted therapy. Nat Rev Endocrinol. 2012;8:486–94.
9. Ng WL, Mohd MT, Shukla K. Functional role of circular RNAs in cancer development and progression. Rna Biol. 2018;15:995–1005.
10. Lei M, Zheng G, Ning Q, Zheng J, Dong D. Translation and functional roles of circular RNAs in human cancer. Mol Cancer. 2020;19:30.
11. Huang A, Zheng H, Wu Z, Chen M, Huang Y. Circular RNA-protein interactions: functions, mechanisms, and identification. Theranostics. 2020;10:3503–17.
12. Hansen TB, Jensen TI, Clausen BH, Bramsen JB, Finsen B, Damgaard CK, et al. Natural RNA circles function as efficient microRNA sponges. Nature. 2013;495:384–8.
13. Du Q, Hu B, Feng Y, Wang Z, Wang X, Zhu D, et al. circOMA1-mediated miR-145-5p suppresses tumor growth of nonfunctioning pituitary adenomas by targeting TPT1. J Clin Endocrinol Metab. 2019;104:2419–34.
14. Abdelmohsen K, Panda AC, Munk R, Grammatikakis I, Dudekula DB, De S, et al. Identification of HuR target circular RNAs uncovers suppression of PABPN1 translation by CircPABPN1. RNA Biol. 2017;14:361–9.
15. Du WW, Fang L, Yang W, Wu N, Awan FM, Yang Z, et al. Induction of tumor apoptosis through a circular RNA enhancing Foxo3 activity. Cell Death Differ. 2017;24:357–70.
16. Yang ZG, Awan FM, Du WW, Zeng Y, Lyu J, Wu D, et al. The circular RNA interacts with STAT3, increasing its nuclear translocation and wound repair by modulating Dnmt3a and miR-17 function. Mol Ther. 2017;25:2062–74.
17. Legnini I, Di Timoteo G, Rossi F, Morlando M, Briganti F, Sthandier O, et al. Circ-ZNF609 Is a circular RNA that can be translated and functions in myogenesis. Mol Cell. 2017;66:22–37.
18. Yang Y, Gao X, Zhang M, Yan S, Sun C, Xiao F, et al. Novel role of FBXW7 circular RNA in repressing glioma tumorigenesis. J Natl Cancer Inst. 2018;110:304–15.
19. Jagannathan S, Hsu JC, Reid DW, Chen Q, Thompson WJ, Moseley AM, et al. Multifunctional roles for the protein translocation machinery in RNA anchoring to the endoplasmic reticulum. J Biol Chem. 2014;289:25907–24.
20. Cui XA, Zhang H, Palazzo AF. p180 promotes the ribosome-independent localization of a subset of mRNA to the endoplasmic reticulum. PLoS Biol. 2012;10: e1001336.
21. Dhillon AS, Hagan S, Rath O, Kolch W. MAP kinase signalling pathways in cancer. Oncogene. 2007;26:3279–90.
22. Suojun Z, Feng W, Dongsheng G, Ting L. Targeting Raf/MEK/ERK pathway in pituitary adenomas. Eur J Cancer. 2012;48:389–95.

23. Yang G, Xu Y, Chen X, Hu G. IFITM1 plays an essential role in the antiproliferative action of interferon-gamma. Oncogene. 2007;26:594–603.
24. Hatano H, Kudo Y, Ogawa I, Tsunematsu T, Kikuchi A, Abiko Y, et al. IFN-induced transmembrane protein 1 promotes invasion at early stage of head and neck cancer progression. Clin Cancer Res. 2008;14:6097–105.
25. Brass AL, Huang IC, Benita Y, John SP, Krishnan MN, Feeley EM, et al. The IFITM proteins mediate cellular resistance to influenza A H1N1 virus, West Nile virus, and dengue virus. Cell 2009;139:1243–54.
26. Pan Y, Cao F, Guo A, Chang W, Chen X, Ma W, et al. Endoplasmic reticulum ribosome-binding protein 1, RRBP1, promotes progression of colorectal cancer and predicts an unfavourable prognosis. Br J Cancer. 2015;113:763–72.
27. Tsai HY, Yang YF, Wu AT, Yang CJ, Liu YP, Jan YH, et al. Endoplasmic reticulum ribosome-binding protein 1 (RRBP1) overexpression is frequently found in lung cancer patients and alleviates intracellular stress-induced apoptosis through the enhancement of GRP78. Oncogene. 2013;32:4921–31.
28. Hyde M, Block-Alper L, Felix J, Webster P, Meyer DI. Induction of secretory pathway components in yeast is associated with increased stability of their mRNA. J Cell Biol. 2002;156:993–1001.
29. Piovesan D, Minervini G, Tosatto SC. The RING 2.0 web server for high quality residue interaction networks. Nucleic Acids Res. 2016;44:W367–W374.
30. Kristensen LS, Andersen MS, Stagsted L, Ebbesen KK, Hansen TB, Kjems J. The biogenesis, biology and characterization of circular RNAs. Nat Rev Genet. 2019;20:675–91.
31. Zhang L, Hou C, Chen C, Guo Y, Yuan W, Yin D, et al. The role of N(6)-methyladenosine (m(6)A) modification in the regulation of circRNAs. Mol Cancer. 2020;19:105.
32. Guo JU, Agarwal V, Guo H, Bartel DP. Expanded identification and characterization of mammalian circular RNAs. Genome Biol. 2014;15:409.
33. Abe N, Matsumoto K, Nishihara M, Nakano Y, Shibata A, Maruyama H, et al. Rolling circle translation of circular RNA in living human cells. Sci Rep. 2015;5:16435.
34. Chen N, Zhao G, Yan X, Lv Z, Yin H, Zhang S, et al. A novel FLI1 exonic circular RNA promotes metastasis in breast cancer by coordinately regulating TET1 and DNMT1. Genome Biol. 2018;19:218.
35. Yánez DC, Ross S, Crompton T. The IFITM protein family in adaptive immunity. Immunology. 2020;159:365–72.
36. Grow EJ, Flynn RA, Chavez SL, Bayless NL, Wossidlo M, Wesche DJ, et al. Intrinsic retroviral reactivation in human preimplantation embryos and pluripotent cells. Nature. 2015;522:221–5.
37. Deblandre GA, Marinx OP, Evans SS, Majjaj S, Leo O, Caput D, et al. Expression cloning of an interferon-inducible 17-kDa membrane protein implicated in the control of cell growth. J Biol Chem. 1995;270:23860–6.
38. Yu F, Xie D, Ng SS, Lum CT, Cai MY, Cheung WK, et al. IFITM1 promotes the metastasis of human colorectal cancer via CAV-1. Cancer Lett. 2015;368:135–43.
39. Escher TE, Lui AJ, Geanes ES, Walter KR, Tawfik O, Hagan CR, et al. Interaction between MUC1 and STAT1 drives IFITM1 overexpression in aromatase inhibitor-resistant breast cancer cells and mediates estrogen-induced apoptosis. Mol Cancer Res. 2019;17:1180–94.
40. Yang J, Li L, Xi Y, Sun R, Wang H, Ren Y, et al. Combination of IFITM1 knockdown and radiotherapy inhibits the growth of oral cancer. Cancer Sci. 2018;109:3115–28.
41. Savitz AJ, Meyer DI. 180-kD ribosome receptor is essential for both ribosome binding and protein translocation. J Cell Biol. 1993;120:853–63.
42. Liang X, Sun S, Zhang X, Wu H, Tao W, Liu T, et al. Expression of ribosome-binding protein 1 correlates with shorter survival in Her-2 positive breast cancer. Cancer Sci. 2015;106:740–6.
43. Danila DC, Zhang X, Zhou Y, Dickersin GR, Fletcher JA, Hedley-Whyte ET, et al. A human pituitary tumor-derived folliculostellate cell line. J Clin Endocrinol Metab. 2000;85:1180–7.

ACKNOWLEDGEMENTS

This research was supported by the National Natural Science Foundation of China for Young Scholars (grant number 81702479 to XJ), Guangdong Basic and Applied Basic Research Foundation (grant number 2020A151501281 to XJ), Science and Technology Program of Jiangmen, China (grant number 2018630100110019805 to YM), and the Natural Science Foundation of Jiangsu Province (grant number BK20200936 to QD).

AUTHOR CONTRIBUTIONS

WZ, SC, QD, PB, and YC carried out experiments and participated in data analysis, statistical analysis, and manuscript preparation. YM, KS, and ZC collected samples. ZL, WZ, and SC participated in data analysis. ZZ, WZ, and XJ participated in writing and proofreading the manuscript. XJ and XF designed the study, were involved in the whole process, and were guarantors of the integrity of the entire study.

COMPETING INTERESTS

The authors declare no competing interests.

ETHICS APPROVAL AND CONSENT TO PARTICIPATE

Informed consent, including a tissue sharing clause, was obtained from a family member of the deceased individual before the autopsy. The use of human tissues in the study was approved by the medical ethics committee of Sun Yat-sen University Cancer Center.

ADDITIONAL INFORMATION

Supplementary information The online version contains supplementary material available at https://doi.org/10.1038/s41388-022-02186-0.

Correspondence and requests for materials should be addressed to Xiang Fan or Xiaobing Jiang.